Design of Ultra-compact Graphene-based Superscatterers

Rujiang Li, Bin Zheng, Xiao Lin, Ran Hao, Shisheng Lin, Wenyan Yin, *Fellow, IEEE*, Erping Li, *Fellow, IEEE*, and Hongsheng Chen

arXiv:1602.07765v1 [physics.optics] 25 Feb 2016

***Abstract*—The energy-momentum dispersion relation is a fundamental property of plasmonic systems. In this paper, we show that the method of dispersion engineering can be used for the design of ultra-compact graphene-based superscatterers. Based on the Bohr model, the dispersion relation of the equivalent planar waveguide is engineered to enhance the scattering cross section of a dielectric cylinder. Bohr conditions with different orders are fulfilled in multiple dispersion curves at the same resonant frequency. Thus the resonance peaks from the first and second order scattering terms are overlapped in the deep-subwavelength scale by delicately tuning the gap thickness between two graphene layers. Using this ultra-compact graphene-based superscatterer, the scattering cross section of the dielectric cylinder can be enhanced by five orders of magnitude.**

***Index Terms*—Superscatterers, dispersion engineering, graphene, Mie scattering theory.**

I. Introduction

SUPERSCATTERER is a device that can magnify the scattering cross section of a given object remarkably [1], [2]. This concept was first proposed based on the transformation optics approach, where the scattering cross section of a cylindrical perfect electric conductor (PEC) is enhanced by an anisotropic and inhomogeneous electromagnetic cover [1], [2], [3], [4], [5], [6], [7], [8]. Alternatively, for subwavelength objects, a superscatterer can be designed by the metal-dielectric layers, where the scattering cross section is magnified due to the enhancement of the localized surface plasmons [9], [10]. Besides, the concept of "surface superscatterers" is also proposed, where the scattering cross section of a deep-subwavelength dielectric cylinder is enhanced by a monolayer graphene sheet which is only one atom thick [11], [12]. Moreover, the scattering cross sections of subwavelength superscatterers can be further enhanced by overlapping the resonances from different scattering terms [13], [14], [15], [16], [17], [18], [19], [20]. Since compact superscatterers are more promising in the miniaturization and integration of plasmonic devices, it is quite necessary to design superscatterers by overlapping different resonance peaks in the deep-subwavelength scale.

Besides, inspired by the Bohr quantization condition in quantum mechanics, a Bohr model that relates the localized surface plasmons and propagating surface plasmons has been proposed recently [21]. Based on this geometric interpretation, the superscattering phenomenon can be understood intuitively by the dispersion relation of the equivalent one dimensional planar plasmonic waveguide. Thus it is feasible to tune the scattering cross sections of subwavelength objects and design the corresponding superscatterers by dispersion engineering. Since the energy-momentum dispersion relation is a fundamental property of photonic and plasmonic systems, dispersion engineering has been used to realize various intriguing phenomena in photonic crystals and plasmonic crystals, e.g. slow light [22], spontaneous emission [23], trapped plasmons [24], and plasmon-induced transparency [25].

In this paper, we show that the method of dispersion engineering can be used to design the ultra-compact graphene-based superscatterers, where the sizes of the superscatterers are in the deep-subwavelength scale. By delicately tuning the dispersion relation of the equivalent planar waveguide, the resonance peaks from the first and second order scattering terms are overlapped. Although the optical loss of graphene exists, the scattering cross section of our ultra-compact superscatterer approaches the single channel limit with the enhancement of five orders of magnitude.

This paper is organized as follows. In section II, the applicability of Bohr model to graphene-based structures is shown by taking the dielectric-graphene-air cylindrical structure as an example. In section III, based on the validation of Bohr model when multiple dispersion curves exist simultaneously, the resonance peaks from the first and second order scattering terms are overlapped by engineering the dispersion relation of the equivalent planar waveguide. In section IV, an ultra-compact graphene-based superscatterer is designed by dispersion engineering. Finally, section V is the conclusion.

II. Bohr model for graphene based structures

For the scattering of plasmonic structures, the scattering models can be related to their equivalent one dimensional

Manuscript received August XX, 2015; revised XXXXXX XX, 201X. This work was sponsored by the National Natural Science Foundation of China under Grants No. 61322501, No. 61574127, and No. 61275183, the National Program for Special Support of Top-Notch Young Professionals, the Program for New Century Excellent Talents (NCET-12-0489) in University, the Fundamental Research Funds for the Central Universities, and the Innovation Joint Research Center for Cyber-Physical-Society System.

R. Li, B. Zheng, X. Lin, and H. Chen are with the State Key Laboratory of Modern Optical Instrumentation, Zhejiang University, Hangzhou 310027, China, with the College of Information Science and Electronic Engineering, Zhejiang University, Hangzhou 310027, China, and also with The Electromagnetics Academy of Zhejiang University, Zhejiang University, Hangzhou 310027, China (e-mails: B. Zheng, zhengbin@zju.edu.cn; H. Chen, hansomchen@zju.edu.cn).

R. Hao, S. Lin, W. Yin, E. Li is with the College of Information Science and Electronic Engineering, Zhejiang University, Hangzhou 310027, China (e-mail: E. Li, liep@zju.edu.cn).

Color versions of one or more of the figures in this paper are available online at http://ieeexplore.ieee.org.

Digital Object Identifier

planar waveguide models by Bohr model [21]. According to the Bohr model, if the phase accumulation along an enclosed optical path is an integral number of 2π, namely if the Bohr condition

$$\oint \beta dl = n \cdot 2\pi \tag{1}$$

is satisfied, the scattering cross sections of the plasmonic structures exhibit resonances. At the resonant frequencies, the scattering cross sections are significantly enhanced which demonstrate the occurrences of superscattering phenomena [11]. In Eq. (1), the integer n is the order of resonance, and β is the corresponding propagation constant of the plasmonic mode in equivalent planar waveguide. The integral (or the enclosed optical path) is calculated along the effective circumference of the plasmonic structures, since surface plasmons propagate along the surface between dielectric and plasmonic material with evanescent fields in the perpendicular directions. Specially, if the plasmonic structure is a cylinder or sphere, Bohr condition reduces to

$$\beta R_{\text{eff}} = n, \tag{2}$$

where R_{eff} is the effective radius of the cylindrical or spherical plasmonic structures. It is worth to note that, since the plasmonic field is highly localized on the interface and the penetration depth is usually small compared with the radius of the cylinder or sphere, the propagation constant β of surface plasmons in a curved circumference is approximately equal to that in an equivalent planar waveguide. Meanwhile, the Bohr model is a phenomenological model and the effective radius is usually determined empirically.

Bohr model has been used to interpret the localized surface plasmons supported by layered metal-dielectric structures [21]. Since graphene is also one kind of plasmonic materials, in this section we show that different orders of superscattering supported by graphene-based structures can be interpreted by the Bohr model as well. Besides, due to the high confinement of graphene plasmons and the one atom thick graphene monolayer, graphene provides a suitable alternative to metal to design the ultra-compact superscatterers in the deep-subwavelength scale [26]. In the calculation, graphene layer is modeled as a two dimensional conducting film [27]. The surface conductivity of graphene monolayer is calculated by the Kubo formula

$$\sigma_g(\omega, \mu_c, \tau, T) = \sigma_{\text{intra}} + \sigma_{\text{inter}}, \tag{3}$$

where

$$\sigma_{\text{intra}} = \frac{ie^2 k_B T}{\pi\hbar^2(\omega + i\tau^{-1})}\left[\frac{\mu_c}{k_B T} + 2\ln\left(e^{-\mu_c/k_B T} + 1\right)\right] \tag{4}$$

is due to intraband contribution, and

$$\sigma_{\text{inter}} = \frac{ie^2(\omega + i\tau^{-1})}{\pi\hbar^2}\int_0^\infty \frac{f_d(-\varepsilon) - f_d(\varepsilon)}{(\omega + i\tau^{-1})^2 - 4(\varepsilon/\hbar)^2} d\varepsilon \tag{5}$$

is due to interband contribution [28], [29]. In the above formula, $-e$ is the charge of an electron, $\hbar = h/2\pi$ is the reduced Plank's constant, T is the temperature, μ_c is the chemical potential, $\tau = \mu\mu_c/ev_F^2$ is the carrier relaxation time, μ is the carrier mobility which ranges from 1 000 cm^2/(V·s) to 230 000 cm^2/(V·s) [30], $v_F = c/300$ is the Fermi velocity, $f_d(\varepsilon) = 1/\left[e^{(\varepsilon-\mu_c)/k_B T} + 1\right]$ is the Fermi-Dirac distribution, and k_B is the Boltzmann's constant.

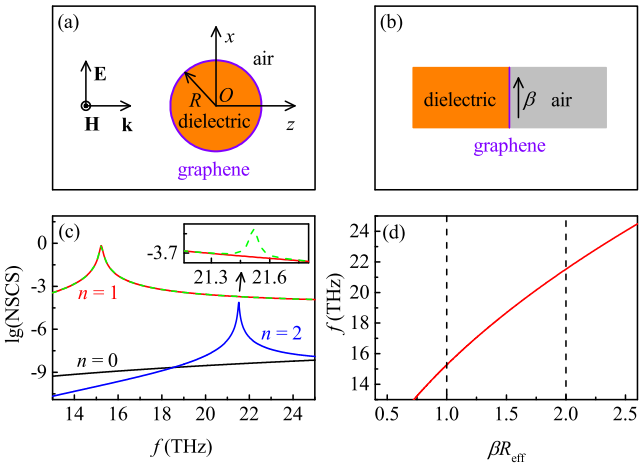

Fig. 1. (Color Online) (a) Cross-sectional view of the layered dielectric-graphene-air cylindrical structure. The dielectric layers are denoted by the orange areas, and the graphene layer is denoted by the violet area. A x-polarized plane wave is incident from air onto the structure. The radius of the cylindrical graphene layer is $R = 250$ nm. (b) Structure of the equivalent planar waveguide model, where the graphene layer (violet area) is separated by a semi-infinite dielectric medium (orange area) and the air (light gray area). The graphene plasmons propagate along the graphene surface in the direction indicated by an arrow, and β is the corresponding propagation constant. (c) The normalized scattering cross sections (NSCSs) at different frequencies for the structure shown in (a), where the dashed green line denotes the total NSCS, while the solid black, red, and blue lines denote contributions from $n = 0$, $n = 1$, and $n = 2$ scattering terms, respectively. The inset is the enlarged figure. Note the NSCSs are expressed in the common logarithmic form. (d) Dispersion relation for the waveguide structure shown in (b). The two vertical dashed black lines indicate the first ($\beta R_{\text{eff}} = 1$) and second ($\beta R_{\text{eff}} = 2$) order Bohr conditions, respectively. The parameters are $\varepsilon_r = 1$, $\mu_r = 1$, $\mu_c = 0.35$ eV, $\mu = 85\,600$ cm^2/(V·s), and $T = 300$ K for (a)-(d).

To demonstrate the applicability of Bohr model to graphene-based structures, we start with a simple case. As shown in Fig. 1(a), a x-polarized plane wave is incident normally from air onto an infinite long graphene coated dielectric cylinder. For simplicity, the relative permittivity of the dielectric cylinder is assumed to be $\varepsilon_r = 1$, and the relative permeability is $\mu_r = 1$. The radius of the cylindrical graphene layer is $R = 250$ nm. Besides, the parameters of the graphene layer are $\mu_c = 0.35$ eV, $\mu = 85\,600$ cm^2/(V·s), and $T = 300$ K. According to the Bohr model, this scattering structure has its equivalent planar waveguide structure as shown in Fig. 1(b), where the graphene layer is separated by a semi-infinite dielectric medium and the air. This planar waveguide supports the propagation of transverse magnetic (TM) surface plasmons, and β is the propagation constant. From Bohr model, the superscattering phenomenon can be understood intuitively by Figs. 1(a) and (b). The incident x-polarized plane wave excites different orders of TM whispering-gallery-like modes along the graphene surface [13], where the modes can be approximated by the TM plasmonic modes in equivalent planar waveguide since the penetration depth of graphene plasmon is smaller than the radius of the cylindrical graphene layer. When one or more whispering-gallery-like modes satisfy the Bohr condition (similar to the whispering gallery condition in

Refs. [13], [14]), the localized electromagnetic fields interfere constructively, and the scattering cross sections are enhanced with resonance peaks accordingly.

For the scattering model in Fig. 1(a), we can calculate the normalized scattering cross section (NSCS) based on the Mie scattering theory [31], [32]. Detailed calculation shows that

$$\text{NSCS} = \sum\nolimits_{n=0}^{\infty} \delta_n \left| s_n \right|^2, \tag{6}$$

where

$$s_n = -\frac{J_n'\left(k_0 R\right) t_n - J_n\left(k_0 R\right) J_n'\left(kR\right)}{H_n^{(1)\prime}\left(k_0 R\right) t_n - H_n^{(1)}\left(k_0 R\right) J_n'\left(kR\right)}, \tag{7}$$

$t_n = \sqrt{\varepsilon_r} J_n\left(kR\right) + i\sigma_g \eta_0 J_n'\left(kR\right)$, $\delta_n = 1$ for $n = 0$ and $\delta_n = 2$ for $n \neq 0$, $k_0 = \omega\sqrt{\varepsilon_0 \mu_0}$ is the wavenumber in free space, $k = k_0\sqrt{\varepsilon_r}$ is the wavenumber in the dielectric cylinder, and J_n and $H_n^{(1)}$ are the n-th order Bessel function of the first kind and Hankel function of the first kind, respectively [33]. Since the degeneracy between $|s_n|$ and $|s_{-n}|$ are considered in Eq. (6), the NSCS has a single channel limit δ_n for the nth angular momentum channel [13]. While for the waveguide model in Fig. 1 (b), the dispersion relation of TM graphene plasmons is

$$\beta = k_0 \sqrt{1 + \left(\frac{2}{\sigma_{g,i}\eta_0}\right)^2}, \tag{8}$$

where $\eta_0 = \sqrt{\mu_0/\varepsilon_0}$ is the impendence of free space, and $\sigma_{g,i}$ is the imaginary part of surface conductivity of graphene [34]. For simplicity, the real part of surface conductivity is omitted in the calculation of dispersion relations in the whole paper to neglect the optical loss of graphene.

Based on Eqs. (6)-(8), Figs. 1(c) and (d) show the NSCSs at different frequencies and the dispersion relation, respectively. In Fig. 1(c), the dashed green line denotes the total NSCS, while the solid black, red, and blue lines denote contributions from $n = 0$, $n = 1$, and $n = 2$ scattering terms, respectively. The inset is the enlarged figure. Clearly, the total NSCS exhibits two resonance peaks at $f = 15.24$ THz and $f = 21.52$ THz, which are caused by the resonances of $n = 1$ and $n = 2$ scattering terms, respectively. Note the NSCSs are expressed in the common logarithmic form since the resonance peaks are very sharp. For this scattering model, the two resonances correspond to the first and second order Bohr conditions with the effective radius $R_{\text{eff}} = R$, respectively. The effective radius is determined because the field intensity is maximum on the graphene surface. As shown in Fig. 1(d), the two vertical dashed black lines indicate the Bohr conditions of $\beta R_{\text{eff}} = 1$ and $\beta R_{\text{eff}} = 2$, where the corresponding resonant frequencies are $f = 15.27$ THz and $f = 21.52$ THz, respectively. The calculation results from Bohr model agree well with that from the scattering model, which implies that Bohr model is applicable for the interpretation of scattering phenomena of graphene-based structures.

Compared with the calculation result in Ref. [21] where Bohr model is used to interpret the superscattering of a metal nanowire, our results are more resonable due to the much tighter confinement of graphene plasmons [26]. Thus Bohr model demonstrates more advantages in designing ultra-compact graphene-based superscatterers.

III. Dispersion engineering

As discussed in the above section, the scattering cross sections of plasmonic structures exhibit resonances where superscattering occurs at the resonant frequencies. However, this kind of resonances are caused by the resonance of a single scattering term, while the contributions from different scattering terms can be overlapped to further enhance the scattering cross sections [13], [14]. Due to the complexity of scattering models, the genetic algorithm has been used to optimize the superscattering of light where different resonance peaks are overlapped [20]. However, it still lacks an intuitive method to design the superscatterers.

Based on the Bohr model, the scattering model is related to its equivalent planar waveguide model intuitively. Thus, it is possible to enhance the scattering cross sections by engineering the dispersion relations of the equivalent planar waveguides. According to Eqs. (1)-(2), different orders of Bohr conditions must be satisfied at the same frequency to overlap the resonance peaks. This requirement can be fulfilled in a single dispersion curve or multiple dispersion curves.

In Refs. [13], [14], different orders of Bohr conditions are satisfied in a single dispersion curve. The metal-dielectric-metal-dielectric-air planar waveguide supports a flat dispersion curve with a proper choice of the thickness of the dielectric layers. Thus, different scattering terms are overlapped and the scattering cross section is enhanced. Alternatively, in this paper we enhance the scattering cross sections of plasmonic structures from a different approach where Bohr conditions with different orders are fulfilled in multiple dispersion curves.

For simplicity, we consider a layered dielectric-graphene-dielectric-graphene-background cylindrical structure, as shown in Fig. 2(a). A x-polarized plane wave is incident normally from the background onto the structure. The background is a dielectric medium with the relative permittivity ε_b and relative permeability $\mu_b = 1$. The relative permittivities of the inner and outer dielectric layers are ε_1 and ε_2, respectively, and the relative permeabilities are $\mu_1 = \mu_2 = 1$. The radii of the inner and outer cylindrical graphene layers are R_1 and R_2, respectively. Besides, the parameters of the graphene layer are $\mu_c = 0.35$ eV, $\mu = 85\ 600\ \text{cm}^2/(\text{V}\cdot\text{s})$, and $T = 300$ K. Similarly, for the scattering model in Fig. 2(a), the corresponding equivalent planar waveguide structure is shown in Fig. 2(b), where $d = R_2 - R_1$ is the gap thickness between two graphene layers.

For the scattering model in Fig. 2(a), the normalized scattering cross section (NSCS) is

$$\text{NSCS} = \sum\nolimits_{n=0}^{\infty} \delta_n \left| s_n \right|^2, \tag{9}$$

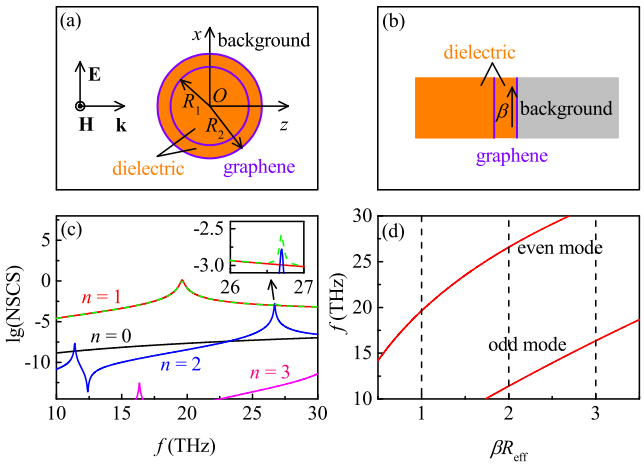

Fig. 2. (Color Online) (a) Cross-sectional view of the layered dielectric-graphene-dielectric-graphene-background cylindrical structure. The dielectric layers are denoted by the orange areas, and the graphene layer is denoted by the violet area. A x-polarized plane wave is incident from background onto the structure. The radii of the inner and outer dielectric layers are R_1 and R_2, respectively. (b) Structure of the equivalent planar waveguide model, where the gap thickness between two graphene layers is $d = R_2 - R_1$. The graphene plasmons propagate along the graphene surface in the direction indicated by an arrow, and β is the corresponding propagation constant. (c) The normalized scattering cross sections (NSCSs) at different frequencies for the structure shown in (a), where the dashed green line denotes the total NSCS, while the solid black, red, blue, and magenta lines denote contributions from $n = 0$, $n = 1$, $n = 2$, and $n = 3$ scattering terms, respectively. The inset is the enlarged figure. Note the NSCSs are expressed in the common logarithmic form. (d) Dispersion relation of graphene plasmons for the waveguide structure shown in (b). The three vertical dashed black lines indicate the first ($\beta R_{\text{eff}} = 1$), second ($\beta R_{\text{eff}} = 2$), and third ($\beta R_{\text{eff}} = 3$) order Bohr conditions, respectively. The parameters are $\varepsilon_1 = \varepsilon_2 = \varepsilon_b = 1$, $\mu_1 = \mu_2 = \mu_b = 1$, $R_1 = 250$ nm, $R_2 = 300$ nm, $d = R_2 - R_1 = 50$ nm, $\mu_c = 0.35$ eV, $\mu = 85\ 600\ \text{cm}^2/(\text{V}\cdot\text{s})$, and $T = 300$ K for (c) and (d).

where

$$s_n = -\frac{J_n'(k_bR_2)\,q_n - \sqrt{\varepsilon_b}J_n(k_bR_2)\,r_n}{H_n^{(1)\prime}(k_bR_2)\,q_n - \sqrt{\varepsilon_b}H_n^{(1)}(k_bR_2)\,r_n}, \tag{10}$$

$$q_n = \sqrt{\varepsilon_2}\left[J_n(k_2R_2) + t_nH_n^{(1)}(k_2R_2)\right] + i\sigma_g\eta_0 r_n, \tag{11}$$

$$r_n = J_n'(k_2R_2) + t_nH_n^{(1)\prime}(k_2R_2), \tag{12}$$

$$t_n = -\frac{J_n'(k_2R_1)\,p_n - \sqrt{\varepsilon_2}J_n(k_2R_1)\,J_n'(k_1R_1)}{H_n^{(1)\prime}(k_2R_1)\,p_n - \sqrt{\varepsilon_2}H_n^{(1)}(k_2R_1)\,J_n'(k_1R_1)}, \tag{13}$$

$$p_n = \sqrt{\varepsilon_1}J_n(k_1R_1) + i\sigma_g\eta_0 J_n'(k_1R_1), \tag{14}$$

and $k_1 = k_0\sqrt{\varepsilon_1}$, $k_2 = k_0\sqrt{\varepsilon_2}$, and $k_b = k_0\sqrt{\varepsilon_b}$ are wavenumbers in the inner and outer dielectric layers, and the background, respectively [31], [32]. While for the waveguide model in Fig. 2(b), the dispersion relation of TM graphene plasmons is

$$e^{-2k_2d} = \frac{\frac{k_2}{\varepsilon_2}\left(1 + i\sigma_g\frac{k_b}{\omega\varepsilon_0\varepsilon_b}\right) + \frac{k_b}{\varepsilon_b}\frac{k_2}{\varepsilon_2}\left(1 + i\sigma_g\frac{k_1}{\omega\varepsilon_0\varepsilon_1}\right) + \frac{k_1}{\varepsilon_1}}{\frac{k_2}{\varepsilon_2}\left(1 + i\sigma_g\frac{k_b}{\omega\varepsilon_0\varepsilon_b}\right) - \frac{k_b}{\varepsilon_b}\frac{k_2}{\varepsilon_2}\left(1 + i\sigma_g\frac{k_1}{\omega\varepsilon_0\varepsilon_1}\right) - \frac{k_1}{\varepsilon_1}}. \tag{15}$$

Speically, when $\varepsilon_1 = \varepsilon_b$, this waveguide is a symmetric double-channel graphene plasmon waveguide, and the dispersion relation reduces to

$$\tanh\left(\frac{k_2d}{2}\right) = -\frac{k_1\varepsilon_2}{k_2\varepsilon_1\left(1 - \sigma_{g,i}\frac{k_1}{\omega\varepsilon_0\varepsilon_1}\right)} \tag{16}$$

for the odd mode, and

$$\tanh\left(\frac{k_2d}{2}\right) = -\frac{k_2\varepsilon_1\left(1 - \sigma_{g,i}\frac{k_1}{\omega\varepsilon_0\varepsilon_1}\right)}{k_1\varepsilon_2} \tag{17}$$

for the even mode [35]. Note the odd and even modes are defined according to the parity of the tangential electric component E_x.

Based on Eqs. (9)-(17), we can tune the positions of the resonance peaks from different scattering terms by dispersion engineering. However, before the demonstration of dispersion engineering, first we need to validate the applicability of Bohr model when multiple dispersion curves exist simultaneously. We consider the simplest case with $\varepsilon_1 = \varepsilon_2 = \varepsilon_b = 1$, $R_1 = 250$ nm, $R_2 = 300$ nm, and $d = R_2 - R_1 = 50$ nm. Under these parameters, Figs. 2(c) and (d) show the NSCSs at different frequencies and the dispersion relation, respectively. In Fig. 2(c), the dashed green line denotes the total NSCS, while the solid black, red, blue, and magenta lines denote contributions from $n = 0$, $n = 1$, $n = 2$, and $n = 3$ scattering terms, respectively. The inset is the enlarged figure. Clearly, the total NSCS exhibits four resonance peaks, where the peak at $f = 19.62$ THz is caused by the resonance of $n = 1$ scattering term, the peaks at $f = 11.40$ THz and $f = 26.70$ are caused by the resonances of $n = 2$ scattering term, and the peak at $f = 16.35$ THz is caused by the resonance of $n = 3$ scattering term, respectively. Note the resonance peaks of total NSCS at $f = 11.40$ THz and $f = 16.35$ THz are not pronounced since the contributions from $n = 2$ and $n = 3$ scattering terms at the corresponding resonant frequencies are small. For this scattering model, these resonances are related to the Bohr conditions with the effective radius $R_{\text{eff}} = (R_1 + R_2)/2$. This effective radius is determined because it corresponds to the bisector of the two graphene layers. As shown in Fig. 2(d), the first order Bohr condition $\beta R_{\text{eff}} = 1$ at $f = 19.63$ THz corresponds to the resonance of $n = 1$ scattering term, the third order Bohr condition $\beta R_{\text{eff}} = 3$ at $f = 16.35$ THz corresponds to the resonance of $n = 3$ scattering term, and the second order Bohr conditions $\beta R_{\text{eff}} = 2$ at $f = 26.58$ THz for the even mode and $f = 11.40$ THz for the odd mode correspond to the resonances of $n = 2$ scattering term at $f = 11.40$ THz and $f = 26.70$ THz, respectively. The calculation results from Bohr model agree well with that from the scattering model, which implies that Bohr model is still applicable when multiple dispersion curves exist simultaneously.

The idea of overlapping the resonance peaks by dispersion engineering is very straightforward. From Fig. 2(d), the dispersion curves of the even mode and odd mode are dependent on the gap thickness d. By delicately tuning the gap thickness, the first order Bohr condition for the even mode and the second order Bohr condition for the odd mode can be fulfilled at the same frequency. In the following calculations, the parameters of the graphene layer are $\mu_c = 1$ eV, $\mu = 230\ 000\ \text{cm}^2/(\text{V}\cdot\text{s})$,

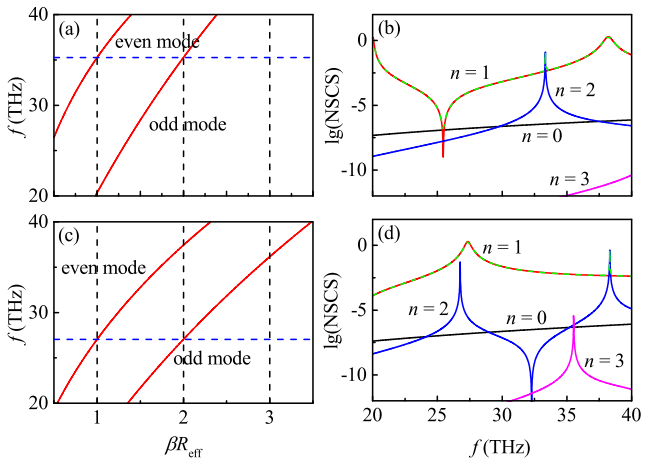

Fig. 3. (Color Online) Left panel: Dispersion relations of graphene plasmons for the waveguide structure shown in Fig. 2(b) with (a) $\varepsilon_1 = \varepsilon_2 = \varepsilon_b = 1$ and $d = 138.20$ nm, and (c) $\varepsilon_1 = \varepsilon_b = 3$, $\varepsilon_2 = 1$, and $d = 44.38$ nm. The three vertical dashed black lines in each figure indicate the first ($\beta R_{\text{eff}} = 1$), second ($\beta R_{\text{eff}} = 2$), and third ($\beta R_{\text{eff}} = 3$) order Bohr conditions, respectively. The resonant frequencies where the resonant peaks are overlapped (indicated by the dashed blue lines) are $f = 35.26$ THz for (a) and $f = 27.04$ THz for (c), respectively. Right panel: The normalized scattering cross sections (NSCSs) at different frequencies for the structure shown in Fig. 2(a) with (b) $\varepsilon_1 = \varepsilon_2 = \varepsilon_b = 1$, $R_1 = 131.54$ nm, and $R_2 = 269.74$ nm, and (d) $\varepsilon_1 = \varepsilon_b = 3$, $\varepsilon_2 = 1$, $R_1 = 122.06$ nm, and $R_2 = 166.43$ nm. In each figure, the dashed green line denotes the total NSCS, while the solid black, red, blue, and magenta lines denote contributions from $n = 0$, $n = 1$, $n = 2$, and $n = 3$ scattering terms, respectively. Note the NSCSs are expressed in the common logarithmic form. The other parameters are $\mu_c = 1$ eV, $\mu = 230\ 000\ \text{cm}^2/(\text{V}\cdot\text{s})$, and $T = 300$ K.

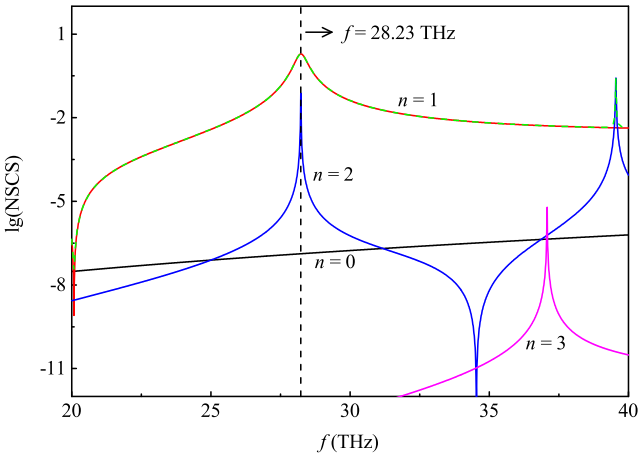

Fig. 4. (Color Online) The normalized scattering cross sections (NSCSs) at different frequencies for the structure shown in Fig. 2(a), where the dashed green line denotes the total NSCS, while the solid black, red, blue, and magenta lines denote contributions from $n = 0$, $n = 1$, $n = 2$, and $n = 3$ scattering terms, respectively. Note the NSCSs are expressed in the common logarithmic form. The parameters are $\varepsilon_1 = \varepsilon_b = 3$, $\varepsilon_2 = 1$, $\mu_1 = \mu_2 = \mu_b = 1$, $R_1 = 112.47$ nm, $R_2 = 160.24$ nm, $\mu_c = 1$ eV, $\mu = 230\ 000\ \text{cm}^2/(\text{V}\cdot\text{s})$, and $T = 300$ K. As indicted by the dashed black line, the resonant frequency where the resonant peaks are overlapped is $f = 28.23$ THz.

and $T = 300$ K to reduce the optical loss of graphene. As shown in Fig. 3(a), when $\varepsilon_1 = \varepsilon_2 = \varepsilon_b = 1$ and the gap thickness $d = 138.20$ nm, the first order Bohr condition for the even mode and the second order Bohr condition for the odd mode are fulfilled at $f = 35.26$ THz. Then we can obtain the radii of the inner and outer graphene layers according to the Bohr condition, namely $R_1 = 131.54$ nm and $R_2 = 269.74$ nm. However, under these parameters the resonance peaks from $n = 1$ and $n = 2$ are not overlapped at $f = 35.26$ THz, as shown in Fig. 3(b). This deviation is due to the invalidation of Bohr model. As shown in Fig. 2(a)-(b), Bohr model relates the scattering model to the waveguide model based on the assumption that the gap thickness d is smaller than the radius of the inner graphene layer. Under this assumption, the excited whispering-gallery-like modes can be approximated by the plasmonic modes in the equivalent one dimensional planar waveguide. For Fig. 3(b), since the gap thickness is nearly equal to the value of R_1, the resonance peaks deviate from the resonant frequency predicted by Bohr model.

In order to fulfill the Bohr condition, we let $\varepsilon_1 = \varepsilon_b = 3$, $\varepsilon_2 = 1$, and $d = 44.38$ nm. Note the background is not air for demonstration purpose. Similarly, as shown in Fig. 3(c), the first order Bohr condition for the even mode and the second order Bohr condition for the odd mode are are fulfilled at $f = 27.04$ THz, and we can obtain $R_1 = 122.06$ nm and $R_2 = 166.43$ nm. Under these parameters, the resonance peaks from $n = 1$ and $n = 2$ are overlapped at $f = 27.04$ THz with a small deviation, as shown in Fig. 3(d). Clearly, Bohr condition is valid since $d < R_1$ in this case. The above result can be optimized further using the simplex search method [36], where $R_1 = 122.06$ nm and $d = 44.38$ nm are set as the initial estimates. This optimization method can find the local optimum values starting at the initial estimates. Fig. 4 show the normalized scattering cross sections (NSCSs) at different frequencies under the optimized values of $R_1 = 112.47$ nm and $R_2 = R_1 + d = 160.24$ nm. Note the resonant frequency slightly changes to $f = 28.23$ THz. Thus the resonant peaks are overlapped by dispersion engineering based on the Bohr model. Note that the total normalized scattering cross section at $f = 28.23$ THz is 2.02, which exceeds the single channel limit of a single scattering term [13]. This implies that it is possible to design the ultra-compact graphene-based superscatterers from an intuitive view.

IV. Design of Superscatterers

In the above section, the resonance peaks are overlapped based on the layered dielectric-graphene-dielectric-graphene-background cylindrical structures. For demonstration purpose, the background is chosen as the dielectric medium with $\varepsilon_b = 3$. Considering the practical applications, the background is the air with $\varepsilon_b = 1$. Thus it is necessary to take this restriction into account when designing the superscatterers. In this section, based on the structure shown in Fig. 2(a) with $\varepsilon_b = 1$, we design an ultra-compact graphene-based superscatterer by dispersion engineering.

Following the similar procedure, we let $\varepsilon_1 = 6$, $\varepsilon_2 = 1.1$, and $\varepsilon_b = 1$, and tune the gap thickness d between two graphene layers. When $d = 63.48$ nm, the first order Bohr condition is fulfilled at $f = 26.30$ THz, the second order Bohr condition is fulfilled at $f = 21.90$ THz, and the radii of the inner graphene layer is $R_1 = 140.623$ nm. Using the

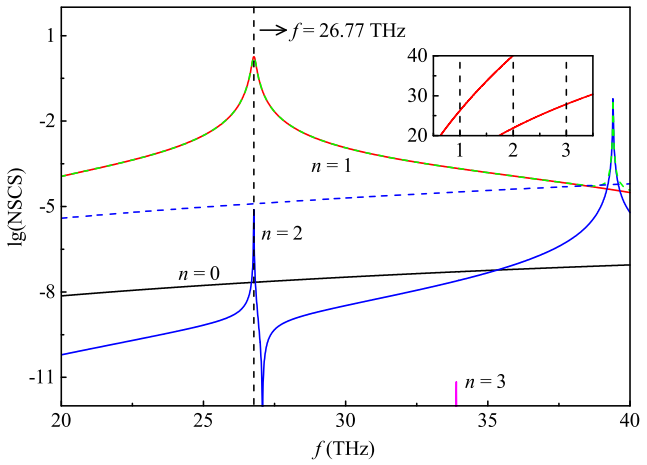

Fig. 5. (Color Online) The normalized scattering cross sections (NSCSs) at different frequencies for the designed superscatterer, where the dashed green line denotes the total NSCS, while the solid black, red, blue, and magenta lines denote contributions from $n = 0$, $n = 1$, $n = 2$, and $n = 3$ scattering terms, respectively. For comparison, the dashed blue line shows the total NSCS of a dielectric cylinder with $R = 118.88$ nm. Note the NSCSs are expressed in the common logarithmic form. The parameters are $\varepsilon_1 = 6$, $\varepsilon_2 = 1.1$, $\varepsilon_b = 1$, $\mu_1 = \mu_2 = \mu_b = 1$, $R_1 = 118.88$ nm, $R_2 = 193.00$ nm, $\mu_c = 1$ eV, $\mu = 230\ 000$ cm$^2/(\mathrm{V}\cdot\mathrm{s})$, and $T = 300$ K. As indicted by the dashed black line, the resonant frequency where the resonant peaks are overlapped is $f = 26.77$ THz. The inset shows the dispersion relation of graphene plasmons in the equivalent planar waveguide.

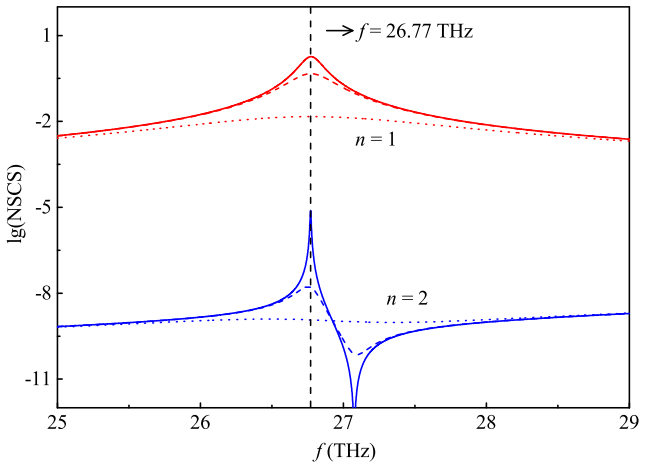

Fig. 6. (Color Online) The normalized scattering cross sections (NSCSs) at different frequencies for the designed superscatterer under different values of carrier mobility of graphene, where the red and blue lines denote contributions from $n = 1$ and $n = 2$ scattering terms, respectively. For simplicity, the curves for $n = 0$ and $n = 3$ are omitted. Note the NSCSs are expressed in the common logarithmic form. The parameters are $\varepsilon_1 = 6$, $\varepsilon_2 = 1.1$, $\varepsilon_b = 1$, $\mu_1 = \mu_2 = \mu_b = 1$, $R_1 = 118.88$ nm, $R_2 = 193.00$ nm, $\mu_c = 1$ eV, $T = 300$ K, $\mu = 230\ 000$ cm$^2/(\mathrm{V}\cdot\mathrm{s})$ for the solid lines, $\mu = 10\ 000$ cm$^2/(\mathrm{V}\cdot\mathrm{s})$ for the dashed lines, and $\mu = 1\ 000$ cm$^2/(\mathrm{V}\cdot\mathrm{s})$ for the dotted lines. As indicted by the dashed black line, the resonant frequency where the resonant peaks are overlapped is $f = 26.77$ THz.

simplex search method, we obtain the optimized values of $R_1 = 118.88$ nm and $R_2 = R_1 + d = 193.00$ nm. Fig. 5 shows the normalized scattering cross sections (NSCSs) at different frequencies, where the resonance peaks are overlapped at the resonant frequency $f = 26.77$ THz. Note that the normalized scattering cross section of a dielectric cylinder with $R = 118.88$ nm is 1.25×10^{-5} at $f = 26.77$ THz, as shown in Fig. 5. Although the total normalized scattering cross section of the superscatterer shown in Fig. 5 is 1.82 which is still under the single channel limit, the scattering cross section contributed by the overlapped resonance peaks has enhanced for five orders of magnitude. Meanwhile, the radius of the ultra-compact superscatterer is only $0.017\lambda_0$, where λ_0 is the incident wavelength. Besides, the optimized values of the superscatterer can be easily obtained by the local optimization algorithm. Compared with the global optimization algorithms, the method of dispersion engineering provides an intuitive way to design the ultra-compact graphene-based superscatterers.

Since the plasmonic field is highly localized on the graphene surface, the superscattering phenomenon is sensitive to the optical loss of graphene. Fig. 6 shows the normalized scattering cross sections (NSCSs) at different frequencies for the designed superscatterer under different values of carrier mobility of graphene. When the carrier mobility decreases, namely the optical loss of graphene increases, the resonant frequency is fixed and the NSCSs from both the $n = 1$ and $n = 2$ scattering terms decrease. Specially, the higher order modes are more susceptible to the optical loss of graphene [12], [13]. This implies that, graphene monolayers with high carrier mobilities are necessary to improve the performance of our ultra-compact graphene-based superscatterers.

Finally, we compare our superscatterers designed by dispersion engineering with those designed using transformation optics. Compared with dispersion engineering, transformation optics is a more general method that can be used to control the scattering of a given object freely. Apart from enhancing the scattering by superscatterers, the scattering can also be suppressed to realize cloaks [37], [38]. Besides, transformation optics can also be used to design electrically-small antennas [39], [40]. These devices are hard to realize by dispersion engineering from an intuitive way. However, superscatterers designed by transformation optics are difficult to implement in experiments since the electromagnetic covers are made of anisotropic and inhomogeneous materials. In contrast, the method of dispersion engineering is more intuitive. More importantly, the superscatterers designed by dispersion engineering are more easier to implement where only isotropic and homogeneous materials are used.

V. Conclusions

In conclusion, based on the validation of Bohr model, we show that the method of dispersion engineering can be introduced to the design of ultra-compact graphene-based superscatterers. Since Bohr conditions with different orders are fulfilled in multiple dispersion curves at the same resonant frequency, the resonance peaks from the first and second order scattering terms are overlapped in the deep-subwavelength scale to further enhance the scattering cross sections by five orders of magnitude. Compared with the global optimization algorithms, our method is more intuitive in physics. Our work will provide theoretical guidance for the design of superscatterers and other scattering based devices, which have great potential applications in plasmonics.

REFERENCES

[1] T. Yang, H. Chen, X. Luo, and H. Ma, "Superscatterer: Enhancement of scattering with complementary media," *Opt. Exp.*, vol. 16, no. 22, pp. 18545-18550, Oct. 2008.

[2] Y. Luo, J. Zhang, H. Chen, B.-I. Wu, and L.-X. Ran, "Wave and ray analysis of a type of cloak exhibiting magnified and shifted scattering effect," *Progress In Electromagnetics Research*, vol. 95, pp. 167-178, 2009.

[3] H. Chen, X. Zhang, X. Luo, H. Ma, and C. T. Chan, "Reshaping the perfect electrical conductor cylinder arbitrarily," *New J. Phys.*, vol. 10, 113016, Nov. 2008.

[4] X. Luo, T. Yang, Y. Gu, H. Chen, and H. Ma, "Conceal an entrance by means of superscatterer," *Appl. Phys. Lett.*, vol. 94, no. 22, 223513, Jun. 2009.

[5] W. H. Wee and J. B. Pendry, "Shrinking optical devices," *New J. Phys.*, vol. 11, 073033, Jul. 2009.

[6] X. Zang, and C. Jiang, "Two-dimensional elliptical electromagnetic superscatterer and superabsorber," *Opt. Exp.*, vol. 18, no. 7, pp. 6891-6899, Mar. 2010.

[7] C. Yang, J. Yang, M. Huang, J. Peng , G. Cai, "Two-dimensional electromagnetic superscatterer with arbitrary geometries," *Comp. Mater. Sci.*, vol. 49, no. 4, pp. 820-825, Oct. 2010.

[8] W. Jiang, B. Xu, Q. Cheng, T. Cui, and G. Yu, "Design and rigorous analysis of transformation-optics scaling devices," *J. Opt. Soc. Am. A*, vol. 30, no. 8, pp. 1698-1702, Aug. 2013.

[9] J. Aizpurua, P. Hanarp, D. S. Sutherland, M. Käll, G. W. Bryant, and F. J. Garcsía de Abajo, "Optical Properties of Gold Nanorings," *Phys. Rev. Lett.*, vol. 90, no. 5, 057401, Feb. 2003.

[10] R. Bardhan, S. Mukherjee, N. A. Mirin, S. D. Levit, P. Nordlander, and N. J. Halas, "Nanosphere-in-a-Nanoshell: A Simple Nanomatryushka," *J. Phys. Chem. C*, vol. 114, no. 16, pp. 7378-7383, Apr. 2010.

[11] R. Li, X. Lin, S. Lin, X. Liu, and H. Chen, "Tunable deep-subwavelength superscattering using graphene monolayers," *Opt. Lett.*, vol. 40, no. 8, pp. 1651-1654, Apr. 2015.

[12] R. Li, X. Lin, S. Lin, X. Liu, and H. Chen, "Atomically thin spherical shell-shaped superscatterers based on a Bohr model," *Nanotechnology*, vol. 26, no. 50, 505201, Nov. 2015.

[13] Z. Ruan and S. Fan, "Superscattering of Light from Subwavelength Nanostructures," *Phys. Rev. Lett.*, vol. 105, no. 1, 013901, Jul. 2010.

[14] Z. Ruan and S. Fan, "Design of subwavelength superscattering nanospheres," *Appl. Phys. Lett.*, vol. 98, no. 4, 043101, Jan. 2011.

[15] L. Verslegers, Z. Yu, Z. Ruan, P. B. Catrysse, and S. Fan, "From Electromagnetically Induced Transparency to Superscattering with a Single Structure: A Coupled-Mode Theory for Doubly Resonant Structures," *Phys. Rev. Lett.*, vol. 108, 083902, Feb. 2012.

[16] H. L. Chen and L. Gao, "Anomalous electromagnetic scattering from radially anisotropic nanowires," *Phys. Rev. A*, vol. 86, no. 3, 033825, Sep. 2012.

[17] A. Mirzaei, I. V. Shadrivov, A. E. Miroshnichenko, and Y. S. Kivshar, "Cloaking and enhanced scattering of core-shell plasmonic nanowires," *Opt. Exp.*, vol. 21, no. 9, pp. 10454-10459, May. 2013.

[18] Y. Huang and L. Gao, "Superscattering of Light from Core-Shell Nonlocal Plasmonic Nanoparticles," *J. Phys. Chem. C*, vol. 118, no. 51, pp. 30170-30178, Dec. 2014.

[19] W. Wan, W. Zheng, Y. Chen, and Z. Liu, "From Fano-like interference to superscattering with a single metallic nanodisk," *Nanoscale*, vol. 6, no. 15, 9093-9102, May. 2014.

[20] A. Mirzaei, A. E. Miroshnichenko, I. V. Shadrivov, and Y. S. Kivshar, "Superscattering of light optimized by a genetic algorithm," *Appl. Phys. Lett.*, vol. 105, no. 1, 011109, Jul. 2014.

[21] W. Liu, R. F. Oulton, and Y. S. Kivshar, "Geometric interpretations for resonances of plasmonic nanoparticles," *Sci. Rep.*, vol. 5, 12148, Jul. 2015.

[22] T. Baba, "Slow light in photonic crystals," *Nat. Photon.*, vol. 2, pp. 465-473, Aug. 2008.

[23] S. Noda, M. Fujita, and T. Asano, "Spontaneous-emission control by photonic crystals and nanocavities," *Nat. Photon.*, vol. 1, pp. 449-458, Aug. 2007.

[24] T. A. Kelf, Y. Sugawara, J. J. Baumberg, M. Abdelsalam, and P. N. Bartlett, "Plasmonic Band Gaps and Trapped Plasmons on Nanostructured Metal Surfaces," *Phys. Rev. Lett.*, vol. 95, no. 11, 116802, Sep. 2005.

[25] S. Zhang, D. A. Genov, Y. Wang, M. Liu, and X. Zhang, "Plasmon-Induced Transparency in Metamaterials," *Phys. Rev. Lett.*, vol. 101, no. 4, 047401, Jul. 2008.

[26] F. H. L. Koppens, D. E. Chang, and F. J. Garcsía de Abajo, "Graphene Plasmonics: A Platform for Strong Light-Matter Interactions," *Nano Lett.*, vol. 11, no. 8, pp. 3370-3377, Jul. 2011.

[27] A. H. Castro Neto, F. Guinea, N. M. R. Peres, K. S. Novoselov, and A. K. Geim, "The electronic properties of graphene," *Rev. Modern phys.*, vol. 81, pp. 109-162, Jan. 2009.

[28] G. W. Hanson, "Dyadic Green's functions and guided surface waves for a surface conductivity model of graphene," *J. Appl. Phys.*, vol. 103, no. 6, 064302, Mar. 2008.

[29] V. P. Gusynin, S. G. Sharapov, and J. P. Carbotte, "Magneto-optical conductivity in graphene," *J. Phys.: Condens. Matter*, vol. 19, no. 2, 026222, Jan. 2007.

[30] W. Gao, J. Shu, C. Qiu, and Q. Xu, "Excitation of Plasmonic Waves in Graphene by Guided-Mode Resonances," *ACS Nano*, vol. 6, no. 9, pp. 7806C7813, Aug. 2012.

[31] A. Ishimaru, *Electromagnetic Wave Propagation, Radiation, and Scattering* (Prentice-Hall, New Jersey, 1991).

[32] C. F. Bohren and D. R. Huffman, *Absorption and Scattering of Light by Small Particles* (Wiley, New York, 1983).

[33] M. Abramowitz and I. A. Stegun, *Handbook of Mathematical Functions with Formulas, Graphs, and Mathematical Tables* (Dover, New York, 1965).

[34] A. Vakil and N. Engheta, "Transformation Optics Using Graphene," *Science*, vol. 332, pp. 1291-1294, Jun. 2011.

[35] S. A. Maier, *Plasmonics: Fundamentals and applications* (Springer, New York, 2007).

[36] J. C. Lagarias, J. A. Reeds, M. H. Wright, and P. E. Wright, "Convergence Properties of the Nelder-Mead Simplex Method in Low Dimensions," *SIAM J. Optimiz.*, vol. 9, no. 1, pp. 112-147, Dec. 1998.

[37] Y. Lai, H. Chen, Z.-Q. Zhang, and C. T. Chan, "Complementary Media Invisibility Cloak that Cloaks Objects at a Distance Outside the Cloaking Shell," *Phys. Rev. Lett.*, vol. 102, no. 9, 093901, Mar. 2009.

[38] J. Zhang, Y. Luo, and N. A. Mortensen, "Hiding levitating objects above a ground plane," *Appl. Phys. Lett.*, vol. 97, no. 13, 133501, Sep. 2010.

[39] Y. Luo, J. Zhang, H. Chen, J. Huangfu, and L. Ran, "High-directivity antenna with small antenna aperture," *Appl. Phys. Lett.*, vol. 95, no. 19, 193506, Nov. 2009.

[40] W. H. Wee and J. B. Pendry, "Super phase array," *New J. Phys.*, vol. 12, 033047, Mar. 2010.

Rujiang Li received the B.S. degree in physics (National Scientific Base for Talented Persons) and M.S. degree in theoretical physics from Shanxi University, Taiyuan, China, in 2011 and 2014, respectively. He is currently working toward the Ph.D. degree in electronic science and technology at Zhejiang University, Hangzhou, China.

His current research interests include scattering by subwavelength structures, nonlinear optics and nonlinear plasmonics, and graphene.

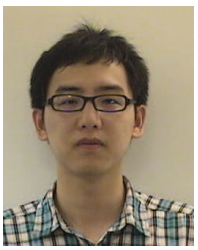

Bin Zheng received the B.S. degree from Ningbo University, Ningbo, China, in 2010; and the Ph.D. degree from Zhejiang University, Hangzhou, China, in 2015. He is currently a postdoctoral researcher in College of Information Science & Electronic Engineering, Zhejiang University, China, since 2015.

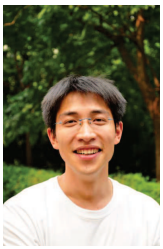

Xiao Lin received the B.S. degree in optical science and engineering from Zhejiang University (ZJU), Hangzhou, China in 2011. He is currently working toward the Ph.D. degree at the college of information science and electronic engineering in ZJU. During his Ph.D. studies, he was a visiting student at the Nanyang Technological University (NTU), Singapore and the Massachusetts Institute of Technology (MIT), USA, respectively. His current interest includes 2D materials, surface plasmons, and electromagnetic radiation.

Ran Hao received his Ph.D. degree in physics from University Paris XI, France in December, 2010. And he received his second Ph.D. degree in Photonics from Wuhan National Laboratory for optoelectronics, Huazhong University of Science & Technology, China, in 2011. He is currently an associate professor in College of information science & electronic engineering, Zhejiang University, China. He has won the Distinguished Young Scholar award in 2011, the Excellent Young Faculty Awards Program in 2012 and 2013, and the Young Scientist Award from the General Assembly and Scientific Symposium of International Union of Radio Science in 2014. His current research interests include plasmonics, nanophotonics, photonic crystals, and graphene photonics. Dr. Hao is a senior member of IEEE photonic society and member of the OSA, SPIE and COS.

Shisheng Lin received his Ph. D. degree in Materials Physics & Chemistry under the joint education of Zhejiang University and Georgia Institute of Technology, in 2010. He is currently an Associate Professor in Zhejiang University. Prof. Lin focused on doping physics in ZnO and its based optoelectronic devices, fabrication and Raman physics of graphene, graphene based optoelectronic devices, 2D materials based metamaterials and energy harvesting devices. Prof. Lin has published more than 50 international refereed journal papers with over 700 times citations.

Wenyan Yin (M'99-SM'01-F'13) received the M.S. degree from Xidian University, Xi'an, China, in 1989, and the Ph.D. degree in electrical engineering from Xi'an Jiao Tong University, Xi'an, China, in 1994. From 1993 to 1996, he was an Associate Professor in Northwestern Polytechnic University, Xi'an, China. From 1996 to 1998, he was a Research Fellow in Duisburg University, Duisburg, Germany. Since 1998, he has been with the National University of Singapore, Singpore, as a Research Scientist and the Project Leader. Since 2005, he has been a Professor in Shanghai Jiao Tong University, Shanghai, China, where he is currently an Adjunct Ph.D. Candidate Supervisor. In 2009, he joined Zhejiang University, China, as a Qiu Shi Distinguished Professor. He has written more than 200 international journal papers. His main research interests are passive and active RF and millimeter-wave device and circuit modeling, ultra-wideband interconnects and signal integrity, nanoelectronics, electromagnetic compatibility (EMC) and electromagnetic protection of communication platforms, and computational multi-physics and its application.

Dr. Yin is an associate editor for the IEEE Transactions on Components, Packaging, and Manufacturing Technology. From 2011 to 2012, he was an IEEE EMC Society Distinguished Lecturer. Since 2013, he has been the IEEE EMC Society Chapter Chair. Since 2011, he has been an associate editor of the International Journal of Electronic Networks, Devices, and Fields. He is also an Editorial Board member of International Journal of RF and Microwave Computer-Aided Engineering. He was the recipient of the the National Technology Invention Award of the Second Class from the Chinese Government in 2008.

Erping Li (S'91-M'92-SM'01-F'08) received the Ph.D. Degree in electrical engineering from Sheffield Hallam University, Sheffield, U.K, in 1992. From 1993 to 1999, he was a Senior Research Fellow, Principal Research Engineer, Associate Professor and the Technical Director at the Singapore Research Institute and Industry. In 2000, he joined the Singapore National Research Institute of High Performance Computing as a Principal Scientist and Director of the Electronic and Photonics Dept. He also holds the Distinguished Professor at Zhejiang University. He authored or co-authored over 400 papers published in the referred international journals and conferences, authored two books. His research interests include electrical modeling and design of micro/nano-scale integrated circuits, 3D electronic package integration and nano-plasmonic technology.

Dr. Li is a Fellow of IEEE, and a Fellow of MIT Electromagnetics Academy, USA. He received numerous awards including the IEEE EMC Richard Stoddard Award for outstanding performance, He has served as an Associate Editor for number of IEEE Transactions and Letters. He has served as a General Chair and Technical Chair, for many international conferences. He was the founding General Chair for the 2008, 2010 and 2012 Asia-Pacific EMC Symposium. He has been invited to give numerous invited talks and plenary speeches at various international conferences and forums.

Hongsheng Chen is a Chang Jiang Scholar Distinguished Professor in the Electromagnetics Academy at Zhejiang University in Hangzhou, Zhejiang, China. He received the B.S. degree in 2000, and Ph.D. degree in 2005, from Zhejiang University, both in electrical engineering.

In 2005, Chen became an Assistant Professor at Zhejiang University; in 2007 an Associate Professor; and in 2011 a Full Professor. In 2014, he was honored with the distinguished "Chang Jiang Scholar" professorship by the Chinese Ministry of Education. He was a Visiting Scientist (2006-2008), and a Visiting Professor (2013-2014) with the Research Laboratory of Electronics at Massachusetts Institute of Technology, USA. His current research interests are in the areas of metamaterials, antennas, invisibility cloaking, transformation optics, graphene, and theoretical and numerical methods of electromagnetics. He is the coauthor of more than 130 international refereed journal papers. His works have been highlighted by many scientific magazines and public media, including Nature, Scientific American, MIT Technology Review, Physorg, and so on. He serves as a regular reviewer of many international journals on electromagnetics, physics, optics, and electrical engineering. He serves on the Topical Editor of Journal of Optics, the Editorial Board of the Nature's Scientific Reports, and Progress in Electromagnetics Research.

Dr. Chen was a recipient of National Excellent Doctoral Dissertation Award in China (2008), the Zhejiang Provincial Outstanding Youth Foundation (2008), the National Youth Top-notch Talent Support Program in China (2012), the New Century Excellent Talents in University of China (2012), and the National Science Foundation for Excellent Young Scholars of China (2013). His research work on invisibility cloak was selected in Science Development Report as one of the representative achievements of Chinese Scientists in 2007.